

# The Inverse Amplitude Method and Chiral Perturbation Theory to two Loops

Torben Hannah\*

*Institute of Physics and Astronomy, Aarhus University, DK-8000 Aarhus C, Denmark*

## Abstract

The inverse amplitude method is analysed to two-loop order in the chiral expansion in the case of  $\pi\pi$  scattering and the pion form factors. The analysis is mainly restricted to the elastic approximation but the possible extension to the inelastic case is also discussed in some detail. It is shown how the two-loop approach improves the inverse amplitude method applied to one-loop order in the chiral expansion. For both  $\pi\pi$  scattering and the pion form factors, it is in fact found that the inverse amplitude method to two-loop order agrees remarkably well with the experimental data up to energies where inelasticities become essential. At somewhat lower energies, the two-loop approach compares well with the one-loop approximation, and in the threshold region they both agree with chiral perturbation theory. This suggests that the inverse amplitude method is indeed a rather systematic way of improving chiral perturbation theory order by order in the chiral expansion.

PACS number(s): 13.75.Lb, 11.30.Rd, 11.55.Fv, 13.40.Gp

Typeset using REVTeX

---

\*Electronic address: hannah@dfi.aau.dk

## I. INTRODUCTION

The effective field theory of QCD, called chiral perturbation theory (ChPT) [1–3], has become a very successful methodology for low-energy hadron physics. This effective field theory is based upon the Goldstone character of the low-lying pseudoscalar mesons and incorporates the appropriate symmetries of the strong interaction. In this approach, one obtains a systematic expansion in powers of external momentum and light quark masses, or equivalently in the number of loops. However, in order to be renormalized order by order, additional low-energy constants have to be introduced at each order in the chiral expansion. These low-energy constants are not fixed by chiral symmetry alone but have to be determined phenomenologically.

At one-loop order in the chiral expansion only a small number of low-energy constants have to be introduced [2]. These are known rather accurately [2,4] and have been used in order to relate different observables to each other. Therefore, one-loop ChPT provides finite predictions for many different low-energy observables in terms of only a very limited amount of empirical input. Even though this has been remarkably successful, the two-loop corrections are important in order to improve the accuracy of the predictions. However, two-loop computations are very laborious and have until now only been accomplished in a limited number of cases. Furthermore, the total number of low-energy constants increases dramatically at this order in the chiral expansion [5]. Since an extensive phenomenological analysis of these new two-loop low-energy constants is not available at present, they have so far been evaluated either from the given process or from underlying models.

Since ChPT provides a systematic perturbative expansion in powers of external momentum and light quark masses, it will satisfy unitarity perturbatively. This implies that the deviation from exact unitarity at a given order provides an estimate of the energy range where the truncation of the chiral expansion is applicable, i.e. the energy range where higher order corrections can be neglected. Although these higher order corrections could in principle be calculated and thereby increase the energy range of the chiral expansion, ChPT is in practice limited to the first few powers in the loop expansion. This is due to the rapid increase in both computational effort and new low-energy constants at each additional order. Thus, the unitarity restriction will give a major limitation on the applicability of ChPT. An important special case of this fact is in the presence of resonances where higher order unitarity corrections become essential.

Therefore, in order to extend the range of applicability of ChPT, unitarity will be of the utmost importance. A rather general way to impose unitarity on the chiral expansion is by the inverse amplitude method (IAM) [6–10], which can be justified by the use of unitarity in a dispersive approach. Since this method combines unitarity and dispersion relations with the chiral expansion, it is likely that it will be more powerful than ChPT alone. The IAM applied to one-loop order in the chiral expansion has been extensively analysed [6–10] and has indeed proven to be a successful method to extend the range of applicability of one-loop ChPT. However, the IAM is not restricted to the one-loop approximation but can in general be applied to any given order in the chiral expansion. Therefore, it might well be that the IAM applied to a given order can be improved by applying it to the next order. If this turns out to be the case, the IAM could be considered as a systematic way of improving ChPT order by order in the chiral expansion.

The IAM was originally applied to  $\pi\pi$  scattering and the pion form factors to one loop in ChPT [6,7]. By now, the full two-loop  $\pi\pi$  scattering amplitude has been evaluated by a dispersive analysis [11] and a field theory calculation [12], respectively. The pion form factors have also been evaluated to two loops some time ago [13]. Therefore, it is now possible to apply the IAM to two loops in the chiral expansion for both  $\pi\pi$  scattering and the pion form factors. In the present paper, this extension of the IAM is analysed and compared to both the one-loop case and one- and two-loop ChPT in order to study whether the IAM is a systematic way of improving ChPT. Section II is devoted to  $\pi\pi$  scattering, Sec. III to the pion form factors, and the conclusions are given in Sec. IV.

## II. $\pi\pi$ SCATTERING

$\pi\pi$  scattering is of fundamental theoretical importance, both because it only involves the self-interaction of the lightest strongly interacting particle, and because it plays a significant role for low-energy hadron phenomenology. The  $\pi\pi$  scattering amplitude can be expressed in terms of a single function  $A(s, t, u)$  as

$$T^{cd;ab}(s, t, u) = \delta^{ab}\delta^{cd}A(s, t, u) + \delta^{ac}\delta^{bd}A(t, s, u) + \delta^{ad}\delta^{bc}A(u, t, s) \quad (1)$$

where  $s = (p^a + p^b)^2$ ,  $t = (p^c - p^a)^2$ , and  $u = (p^d - p^a)^2$  are the Mandelstam variables. The definite isospin amplitudes  $T^I$  are given in terms of the function  $A(s, t, u)$  as

$$\begin{aligned} T^0(s, t, u) &= 3A(s, t, u) + A(t, s, u) + A(u, t, s), \\ T^1(s, t, u) &= A(t, s, u) - A(u, t, s), \\ T^2(s, t, u) &= A(t, s, u) + A(u, t, s), \end{aligned} \quad (2)$$

and the projection of these isospin amplitudes onto partial waves is given by

$$t_l^I(s) = \frac{1}{64\pi} \int_{-1}^1 d(\cos\theta) P_l(\cos\theta) T^I(s, t, u). \quad (3)$$

In the elastic region  $4M_\pi^2 < s < 16M_\pi^2$ , unitarity implies that the partial waves satisfy the following relation

$$\text{Im}t_l^I(s) = \sigma(s)|t_l^I(s)|^2 \quad (4)$$

where  $\sigma = \sqrt{(s - 4M_\pi^2)/s}$  is the phase-space factor. As a consequence of Eq. (4), the partial waves can be parametrized in terms of real phase shifts  $\delta_l^I$  as

$$t_l^I(s) = \frac{1}{\sigma(s)} \frac{1}{2i} \left\{ \exp[i2\delta_l^I(s)] - 1 \right\}. \quad (5)$$

The elastic unitarity relation (4) is in practice useful up to the  $K\bar{K}$  threshold [14]. Above this energy the extended unitarity relation becomes

$$\text{Im}t_l^I(s) = \sigma(s)|t_l^I(s)|^2 + \sigma_{(K)}(s)|t_{l(K)}^I(s)|^2 \quad (6)$$

where  $t_{(K)}$  is the partial wave for the process  $\pi\pi \rightarrow K\bar{K}$  and  $\sigma_{(K)}$  is the corresponding phase-space factor. At still higher energies, other important inelastic channels must be included and the unitarity relation has to be generalized further. The inelastic channels can be included in the parametrization (5) by adding an imaginary part to the phase shifts.

## A. Chiral perturbation theory

In the framework of ChPT, the  $\pi\pi$  scattering amplitude is obtained as an expansion in powers of external momentum and light quark masses

$$A(s, t, u) = A^{(0)}(s, t, u) + A^{(1)}(s, t, u) + A^{(2)}(s, t, u) + \dots \quad (7)$$

where  $A^{(n)}$  is of  $O(p^{2n+2})$ . The leading order term  $A^{(0)}$  corresponds to the current algebra result derived by Weinberg [15], whereas  $A^{(1)}$  is the one-loop correction determined by Gasser and Leutwyler [2]. Recently, the two-loop correction  $A^{(2)}$  has also been evaluated by a dispersive analysis [11] and a field theory calculation [12], respectively. These two approaches agree insofar as the general structure of the amplitude is concerned. However, the field theory calculation contains additional information regarding the dependence of the chiral low-energy constants which is not obtained in the dispersive analysis.

The full  $\pi\pi$  scattering amplitude to two loops in ChPT is given in Ref. [12] where the contributions of  $O(p^8)$  have been omitted here. At one-loop order, there are four low-energy constants  $l_1^r, l_2^r, l_3^r,$  and  $l_4^r$ , whereas six additional low-energy constants  $r_1^r, r_2^r, r_3^r, r_4^r, r_5^r,$  and  $r_6^r$  have to be introduced at two-loop order. The superscript  $r$  indicates that these low-energy constants depend on the renormalization scale  $\mu$ , whereas the full amplitude is scale independent. The projection onto partial waves of the chiral  $\pi\pi$  scattering amplitude (7) gives the following expansion

$$t_l^I(s) = t_l^{I(0)}(s) + t_l^{I(1)}(s) + t_l^{I(2)}(s) + \dots \quad (8)$$

These partial waves will satisfy the elastic unitarity relation (4) perturbatively, i.e. one has to two-loop order

$$\begin{aligned} \text{Im}t_l^{I(0)}(s) &= 0, \\ \text{Im}t_l^{I(1)}(s) &= \sigma(s)t_l^{I(0)2}(s), \\ \text{Im}t_l^{I(2)}(s) &= \sigma(s)2t_l^{I(0)}(s)\text{Re}t_l^{I(1)}(s). \end{aligned} \quad (9)$$

The first inelastic channel is the four pion intermediate state, which is a three-loop effect of  $O(p^8)$ . Other inelastic channels with more pions are of even higher order in the chiral expansion. This implies that the perturbative elastic unitarity relations to two loops will hold at least up to the  $K\bar{K}$  threshold. In fact, in the framework of SU(2) ChPT the relations (9) are satisfied for all energies above threshold, whereas in SU(3) ChPT they have to be generalized above the  $K\bar{K}$  and  $\eta\eta$  thresholds. The generalization above the  $K\bar{K}$  threshold is obtained from the perturbative interpretation of Eq. (6)

$$\begin{aligned} \text{Im}t_l^{I(0)}(s) &= 0, \\ \text{Im}t_l^{I(1)}(s) &= \sigma(s)t_l^{I(0)2}(s) + \sigma_{(K)}(s)t_{l(K)}^{I(0)2}(s), \\ \text{Im}t_l^{I(2)}(s) &= \sigma(s)2t_l^{I(0)}(s)\text{Re}t_l^{I(1)}(s) + \sigma_{(K)}(s)2t_{l(K)}^{I(0)}(s)\text{Re}t_{l(K)}^{I(1)}(s). \end{aligned} \quad (10)$$

The further extension of these perturbative relations above the  $\eta\eta$  threshold is obtained in a straightforward manner.

## B. Inverse amplitude method

The two-loop  $\pi\pi$  scattering amplitude has hitherto only been evaluated within the framework of SU(2) ChPT [11,12]. This implies that in the derivation of the IAM applied to two loops in the chiral expansion, the elastic approximation is used. However, the limitations of this approximation and the possible extension to SU(3) ChPT will also be discussed in some detail.

### 1. Elastic approximation

From the fundamental principles of S matrix theory, it can be shown that the  $\pi\pi$  partial waves are analytic in the complex  $s$  plane with a right or unitarity cut for  $4M_\pi^2 < s < \infty$  and a left cut for  $-\infty < s < 0$ . Therefore, the  $\pi\pi$  partial waves can be expressed in terms of dispersion relations with a number of subtractions to ensure the convergence of the integrals. The same is also true for the inverse of the partial waves or more exactly for the function  $\Gamma = t^{(0)2}/t$ . Neglecting possible pole contributions arising from zeros in the partial waves [7], the four times subtracted dispersion relation for the IAM is

$$\Gamma(s) = \Gamma_0 + \Gamma_1 s + \Gamma_2 s^2 + \Gamma_3 s^3 + \frac{s^4}{\pi} \int_{4M_\pi^2}^{\infty} \frac{\text{Im}\Gamma(s') ds'}{s'^4 (s' - s - i\epsilon)} + \frac{s^4}{\pi} \int_{-\infty}^0 \frac{\text{Im}\Gamma(s') ds'}{s'^4 (s' - s - i\epsilon)}. \quad (11)$$

Four subtractions are used in order to ensure that two-loop ChPT satisfies a similar dispersion relation. On the right cut, the elastic unitarity relation (4) gives  $\text{Im}\Gamma = -t^{(0)2} \text{Im}t/|t|^2 = -\sigma t^{(0)2}$ , i.e. this part can be computed exactly. The same is not true for the left cut, which, however, can be approximated by means of two-loop ChPT. Expanding the function  $\Gamma$  to two loops in the chiral expansion  $\Gamma = t^{(0)} - t^{(1)} + t^{(1)2}/t^{(0)} - t^{(2)}$ , one finds that the left cut can be approximated by  $\text{Im}\Gamma = -\text{Im}t^{(1)} + 2\text{Ret}^{(1)} \text{Im}t^{(1)}/t^{(0)} - \text{Im}t^{(2)}$ . Finally, the subtraction constants can also be evaluated to two-loop order in the chiral expansion. Denoting these subtraction constants  $a_0, a_1, a_2$ , and  $a_3$ , the following dispersion relation is obtained for the IAM

$$\frac{t_l^{I(0)2}(s)}{t_l^I(s)} = a_0 + a_1 s + a_2 s^2 + a_3 s^3 - \frac{s^4}{\pi} \int_{4M_\pi^2}^{\infty} \frac{\sigma(s') t_l^{I(0)2}(s') ds'}{s'^4 (s' - s - i\epsilon)} - \frac{s^4}{\pi} \int_{-\infty}^0 \frac{[\text{Im}t_l^{I(1)}(s') - 2\text{Ret}_l^{I(1)}(s') \text{Im}t_l^{I(1)}(s')/t_l^{I(0)}(s') + \text{Im}t_l^{I(2)}(s')] ds'}{s'^4 (s' - s - i\epsilon)}. \quad (12)$$

This dispersion relation implies that the partial wave  $t$  can be obtained from the two-loop chiral expansion. However, the relation between the IAM and two-loop ChPT can be simplified by writing down a four-subtracted dispersion relation for the function  $\Gamma^{(2)} = t^{(0)} - t^{(1)} + t^{(1)2}/t^{(0)} - t^{(2)}$ . Since this is the function  $\Gamma$  expanded to two-loop order, the left cut and subtraction constants in the dispersion relation for  $\Gamma^{(2)}$  will be the same as in Eq. (12). For the right cut, the perturbative elastic unitarity relations (9) imply that  $\text{Im}\Gamma^{(2)} = -\text{Im}t^{(1)} + 2\text{Ret}^{(1)} \text{Im}t^{(1)}/t^{(0)} - \text{Im}t^{(2)} = -\sigma t^{(0)2} + \sigma 2t^{(0)} \text{Ret}^{(1)} - \sigma 2t^{(0)} \text{Ret}^{(1)} = -\sigma t^{(0)2}$ . Thus, the following dispersion relation is obtained

$$\begin{aligned}
t_l^{I(0)}(s) - t_l^{I(1)}(s) + \frac{t_l^{I(1)^2}(s)}{t_l^{I(0)}(s)} - t_l^{I(2)}(s) &= a_0 + a_1 s + a_2 s^2 + a_3 s^3 - \frac{s^4}{\pi} \int_{4M_\pi^2}^{\infty} \frac{\sigma(s') t_l^{I(0)^2}(s') ds'}{s'^4 (s' - s - i\epsilon)} \\
- \frac{s^4}{\pi} \int_{-\infty}^0 \frac{[\text{Im} t_l^{I(1)}(s') - 2\text{Re} t_l^{I(1)}(s') \text{Im} t_l^{I(1)}(s') / t_l^{I(0)}(s') + \text{Im} t_l^{I(2)}(s')]}{s'^4 (s' - s - i\epsilon)} ds', & \quad (13)
\end{aligned}$$

which is exactly the same as in Eq. (12). Therefore, the IAM to two loops in the chiral expansion gives the partial wave  $t$  in the simple form

$$t_l^I(s) = \frac{t_l^{I(0)}(s)}{1 - t_l^{I(1)}(s)/t_l^{I(0)}(s) + t_l^{I(1)^2}(s)/t_l^{I(0)^2}(s) - t_l^{I(2)}(s)/t_l^{I(0)}(s)}. \quad (14)$$

Since this is formally equivalent to the [0,2] Padé approximant applied on ChPT, the expression (14) will coincide with the chiral expansion up to two-loop order. However, in deriving (14) two-loop ChPT has only been used for the left cut and the subtraction constants, whereas the important unitarity cut was computed exactly. This is in contrast to ChPT where the unitarity cut was only computed perturbatively. As a consequence of this, the [0,2] Padé approximant (14) satisfies the elastic unitarity relation (4) exactly and not only perturbatively as in ChPT.

The IAM can in general be applied to any given order in the chiral expansion, but has up to now almost entirely been restricted to the one-loop approximation [6–10]. In this case, the IAM gives the partial waves in the form

$$t_l^I(s) = \frac{t_l^{I(0)}(s)}{1 - t_l^{I(1)}(s)/t_l^{I(0)}(s)}, \quad (15)$$

which is formally equivalent to the [0,1] Padé approximant. This form also satisfies unitarity exactly and coincides with the chiral expansion up to one-loop order. It is derived in the same way as described above, the only difference being that the left cut and subtraction constants in Eq. (12) are now approximated only to one-loop order in the chiral expansion. This shows how the IAM to two loops improves the IAM to one loop, even though the dominantly unitarity cut is computed exactly in both cases.

The above discussion rests upon the assumption that the leading order term  $t^{(0)}$  does not vanish. In fact, this is only true for the lowest partial waves with  $l \leq 1$ , whereas the higher partial waves start at one-loop order in the chiral expansion. In these cases, the IAM must be slightly modified by writing down a dispersion relation for the function  $t^{(1)^2}/t$ . Since perturbative unitarity implies that  $t^{(1)}$  is real on the right cut for these higher partial waves, the elastic unitarity relation (4) gives  $\text{Im}(t^{(1)^2}/t) = -t^{(1)^2} \text{Im}t/|t|^2 = -\sigma t^{(1)^2}$ . Hence, the right cut can also in these cases be computed exactly, whereas the left cut and subtraction constants can be approximated by means of ChPT as above. However, in order to relate the dispersion relation for the IAM to a corresponding one for ChPT, one has to go to three loops in the chiral expansion. This is due to the fact that for the higher partial waves the imaginary part on the right cut starts at  $O(p^8)$  in ChPT. Should such a three-loop calculation be undertaken in the future, the IAM could also in these cases be directly related to ChPT in the same way as discussed above.

## 2. Inclusion of inelasticities

It would be desirable if the IAM could be applied beyond the elastic approximation. The first important inelastic channel in  $\pi\pi$  scattering opens up at the  $K\bar{K}$  threshold and is due to the  $K\bar{K}$  intermediate state. At a slightly higher energy the  $\eta\eta$  inelastic channel will also appear, but this is a rather unimportant effect. Only at still higher energies will the four-pion intermediate state begin to be significant, together with other inelastic channels. The  $K\bar{K}$  and  $\eta\eta$  intermediate states are already present at one-loop order in SU(3) ChPT [16], and will therefore also appear in an extension of the present two-loop calculation to the SU(3) case. Thus, it might be that the IAM applied to two loops in the SU(3) chiral expansion could include these inelasticities. In order to try to include the four-pion intermediate state, one would need to apply the IAM to three loops since this effect is of  $O(p^8)$  in the chiral expansion.

Therefore, the following discussion is restricted to the  $K\bar{K}$  and  $\eta\eta$  inelastic channels. In fact, it will be limited to the important  $K\bar{K}$  case since the extension to the  $K\bar{K}/\eta\eta$  case is rather obvious. To include the  $K\bar{K}$  inelastic channel, the extended unitarity relation (6) has to be used above the  $K\bar{K}$  threshold in computing the right cut in Eq. (12), whereas the other parts are computed in exactly the same way as before. Thus, since the relation (6) gives  $\text{Im}\Gamma = -t^{(0)2}\text{Im}t/|t|^2 = -\sigma t^{(0)2} - \sigma_{(K)}t^{(0)2}|t_{(K)}|^2/|t|^2$ , this expression has to be used above the  $K\bar{K}$  threshold in Eq. (12). However, in this case it is not possible to compute the inelastic part  $|t_{(K)}|^2/|t|^2$  exactly, so this part must be evaluated to two loops in the SU(3) chiral expansion

$$\begin{aligned} \text{Im}\Gamma(s) &= -\sigma(s)t_i^{I(0)2}(s) - \sigma_{(K)}(s)t_i^{I(0)2}(s)\frac{|t_{i(K)}^I(s)|^2}{|t_i^I(s)|^2} \\ &\approx -\sigma(s)t_i^{I(0)2}(s) - \sigma_{(K)}(s)t_{i(K)}^{I(0)2}(s) \\ &\quad -\sigma_{(K)}(s)2t_{i(K)}^{I(0)2}(s)\left[\frac{\text{Re}t_{i(K)}^{I(1)}(s)}{t_{i(K)}^{I(0)}(s)} - \frac{\text{Re}t_i^{I(1)}(s)}{t_i^{I(0)}(s)}\right]. \end{aligned} \quad (16)$$

In order to simplify the relation between the IAM and ChPT for the SU(3) case, the right cut in Eq. (13) has to be evaluated with the inclusion of the  $K\bar{K}$  intermediate state. From the extended perturbative unitarity relations (10), one finds that  $\text{Im}\Gamma^{(2)}$  is given by an expression exactly similar to Eq. (16). Thus, the inelastic case also gives a result of the form (14), the only difference being that in this case the chiral SU(3) expansion is used. In a similar way, by expanding the inelastic part  $|t_{(K)}|^2/|t|^2$  to one-loop order, the IAM gives a result of the form (15) with ChPT evaluated within SU(3).

In the presence of the  $K\bar{K}$  inelasticity, the unitarity cut cannot be computed exactly, but one has to expand the inelastic part to a given chiral order. Since the inelastic part starts at the  $K\bar{K}$  threshold, the one- and two-loop chiral expansions would seem to lead to rather unreliable approximations. However, it is important to realize that for the inelastic IAM the exact extended unitarity relation has been applied before the inelastic part is approximated by the chiral expansion. Furthermore, if one compare the expansion of the inelastic part for the IAM (16) with the corresponding expansion for ChPT (10), the two-loop correction in Eq. (16) is likely to be more suppressed compared to the two-loop correction in Eq.

(10). Therefore, one might expect that the expansion of the inelastic quantity  $|t_{(K)}|^2/|t|^2$  converges rather rapidly, i.e. the one- and two-loop expansion could be used over a large energy range. Indeed, as will be shown in the case of the pion form factors, the expansion of a similar quantity works very well up to rather high energies.

In order to evaluate how well the inelastic IAM agrees with the extended unitarity relation (6), one needs to determine the  $t_{(K)}$  partial waves. To do this, the IAM could be applied to one- and two-loop order for these partial waves. In this way one finds that the inelastic IAM satisfies Eq. (6) exactly, provided that the quantity  $|t_{(K)}|^2/|t|^2$  is determined by the leading order term. Thus, the IAM is a rather consistent approach, but there is of course no way to know a priori to what extent this method can reproduce the inelasticities.

### C. Comparison with experiment

The chiral expansion depends on a number of low-energy constants not fixed by chiral symmetry alone. These have to be determined before ChPT and the IAM can be compared with experimental data. In the present paper, this comparison is limited to the lowest  $\pi\pi$  partial waves with  $l \leq 1$ , since they are the best known experimentally.

#### 1. The low-energy constants

Since the chiral low-energy constants depend on the renormalization scale  $\mu$ , this scale has to be chosen before the low-energy constants can be fixed. This scale will be set at the mass of the  $\rho(770)$  resonance, i.e.  $\mu = M_\rho = 770$  MeV. In addition, throughout this paper the values  $F_\pi = 92.4$  MeV and  $M_\pi = 139.6$  MeV are used for the pion decay constant and pion mass, respectively.

The  $\pi\pi$  partial waves depend on four low-energy constants  $l_1^r$ ,  $l_2^r$ ,  $l_3^r$ , and  $l_4^r$  to one-loop order in the chiral expansion. These have been determined phenomenologically rather accurately in one-loop ChPT [2,4] with results displayed in the first column in Table I. For ChPT to two loops, these low-energy constants should in principle be re-evaluated taking into account the two-loop corrections. However, since a thorough reevaluation seems rather out of reach at the moment, the one-loop values of  $l_1^r$ ,  $l_2^r$ ,  $l_3^r$ , and  $l_4^r$  are also used in two-loop ChPT. The additional low-energy constants to two loops  $r_1^r$ ,  $r_2^r$ ,  $r_3^r$ ,  $r_4^r$ ,  $r_5^r$ , and  $r_6^r$  may be estimated with the assumption that they are dominated by resonance contributions at the scale of the resonance, an assumption that is well satisfied in one-loop ChPT [2,17]. In particular, including contributions from vector and scalar exchange together with terms of  $O(p^6)$  coming from SU(3) one-loop ChPT [12], one obtains the values for these two-loop low-energy constants given in the second column in Table I [18].

The IAM to a given order depends on the same low-energy constants as ChPT to the same order. However, the phenomenological determination of these low-energy constants by the IAM do not necessarily coincide precisely with the values obtained in ChPT. This is due to the fact that the IAM contains higher order unitarity corrections, which will effect the phenomenological determination of the low-energy constants. Some of the low-energy constants in the IAM to one and two loops may be determined phenomenologically by fitting the experimental  $\pi\pi$  phase shifts. In this fitting, the data obtained from  $K_{l4}$  decays [19] are



used together with the data from high statistics medium energy experiments [20–24]. For a recent discussion of the experimental  $\pi\pi$  scattering data see Ref. [25].

The low-energy constants  $l_1^r$  and  $l_2^r$  in the IAM to one loop may be determined in this way, whereas the fit will be rather insensitive to the precise values of the other low-energy constants  $l_3^r$  and  $l_4^r$ . For these latter low-energy constants, the values obtained in one-loop ChPT are also used in the IAM to one loop. In the case of  $l_1^r$  and  $l_2^r$ , one is used to fix the  $\rho(770)$  resonance defined to be at  $\delta_1^1(M_\rho) = \pi/2$ , whereas the other is determined by fitting the  $\delta_0^0$  and  $\delta_0^2$  experimental phase shifts for  $\sqrt{s} \leq 0.7$  GeV. This will give an acceptable fit with values of  $l_1^r$  and  $l_2^r$  given in the third column in Table I, whereas if one increase the energy range to  $\sqrt{s} \leq 0.9$  GeV, the fit will not be acceptable.

However, the IAM to two loops might improve the agreement with the experimental phase shifts up to  $\sqrt{s} = 0.9$  GeV. In this case the fit is mainly sensitive to  $l_1^r$ ,  $l_2^r$ ,  $r_5^r$ , and  $r_6^r$ , so the other low-energy constants will be given by the same values as in two-loop ChPT. With the use of the  $\rho(770)$  resonance to fix  $r_6^r$  and varying  $l_1^r$ ,  $l_2^r$ , and  $r_5^r$  around the values used in two-loop ChPT, these low-energy constants are determined by fitting the  $\delta_0^0$  and  $\delta_0^2$  experimental phase shifts up to  $\sqrt{s} = 0.9$  GeV. In this case one obtains an acceptable fit with values of the low-energy constants given in the fourth column in Table I. There is no point in extending this fit further up in energy since inelastic effects will become essential above approximately 0.9 GeV.

The low-energy constants in Table I have not been assigned any error bars since it is difficult to estimate these error bars taking into account the higher order corrections. In addition, it is not possible to assign reliable error bars on the two-loop low-energy constants estimated from resonance exchange. Nevertheless, from Table I it is observed that the values of the low-energy constants in ChPT and the IAM to both one and two loops are rather consistent with each other. However, some variations are indeed to be expected due to the different treatments of the higher order corrections.

## 2. Threshold parameters and phase shifts

Close to threshold, the  $\pi\pi$  partial waves can be parametrized in terms of scattering lengths  $a_l^I$  and slope parameters  $b_l^I$  [26]. In Table II, the values obtained from ChPT and the IAM are compared to the experimental information for these threshold parameters. It is observed that one-loop ChPT gives relatively large corrections to the leading order current algebra results, whereas the additional two-loop ChPT corrections are somewhat smaller. However, the difference between one and two-loop ChPT is in general larger than the corresponding difference between the IAM to one and two loops, which supports the expectation that the IAM to one loop already includes the most important unitarity corrections. In fact, the IAM to both one and two loops compares remarkably well with two-loop ChPT for the  $I = 0$  S wave, where the unitarity corrections are important even at low energies. For the other channels, where the higher order unitarity corrections are less important at low energies, the IAM compares in general rather well with both one and two-loop ChPT.

Regarding the comparison with the experimental information, both the IAM and ChPT to one and two loops are quite consistent with the data. Unfortunately, the precision of these data does not allow one to distinguish the higher order corrections from the one-loop

contribution, but this might be improved with the forthcoming accurately determination of  $a_0^0 - a_0^2$  from the measurement of the lifetime of the  $\pi^+\pi^-$  atom [28].

Even though the chiral expansion only satisfies unitarity perturbatively, ChPT is not in general restricted to the threshold region. However, the deviation from exact unitarity will give an estimate of the actual energy range where the given truncation of the chiral expansion is applicable. This deviation is shown in the Argand diagrams in Fig. 1 for the three lowest partial waves. This shows that unitarity is indeed improved at low energies at each additional order in the chiral expansion. On the other hand, two-loop ChPT begins to deviate significantly from exact unitarity above approximately 0.5 GeV for all three partial waves. Therefore, two-loop ChPT should only be trusted up to about this energy, whereas the energy range for one-loop ChPT is somewhat smaller.

Despite the fact that ChPT only satisfies unitarity perturbatively, it is possible to define a chiral expansion for the phase shifts  $\delta_l^I$  [11,29]. In Fig. 2, the phase shift difference  $\delta_0^0 - \delta_1^1$  given by the IAM and ChPT is compared to the experimental data obtained from  $K_{l4}$  decays [19]. The IAM to one and two loops gives very similar results in the displayed energy region. Furthermore, since these results compare very well to both two-loop ChPT and the central experimental data, the higher order unitarity corrections are indeed very well approximated by the IAM. As for one-loop ChPT, this appears to be systematically below the central experimental data, although it is still consistent with these data within the error bars. At DAΦNE, it is expected that these error bars can be significantly reduced from new high statistics measurements of the  $K_{l4}$  decays [30]. From this, it will also be possible to determine accurately some of the low-energy constants in the IAM from independent observables [8] and thereby test the consistency of the IAM in great detail.

In Fig. 3, the phase shift  $\delta_0^0$  is shown below  $\sqrt{s} = 1$  GeV. It is observed that the IAM to two loops agrees rather well with the data up to approximately 0.9 GeV, whereas the IAM to one loop only describes the data well up to about 0.7 GeV. For one and two-loop ChPT, both begin to disagree with the data somewhat above 0.5 GeV, which is consistent with the unitarity requirement. In fact, the IAM to two loops describes the data rather well up to energies where the elastic approximation will no longer be applicable. Therefore, before one tries to apply this method to even higher energies, the  $K\bar{K}$  inelasticity must be included in the IAM as discussed previously. However, whether this inelastic IAM will actually be able to reproduce the  $f_0(980)$  resonance, which is closely related to the  $K\bar{K}$  inelastic channel, has to await further investigations.

In Fig. 4, the phase shift  $\delta_0^2$  is shown below  $\sqrt{s} = 1.4$  GeV. In this case, the IAM to two loops also seems to improve the IAM to one loop at higher energies, even though the data are not very conclusive. In addition, the IAM also in this case successfully extends the range of applicability of ChPT. In this channel, the first important inelastic effect is due to the four pion intermediate state, which should begin to be significant somewhat above 1.2 GeV. Thus, the IAM to two loops describes the data well up to energies where this inelasticity should be included. It also seems that two-loop ChPT is rather consistent with the data all the way up to about 1 GeV. However, this is in conflict with the unitarity requirement, which shows that two-loop ChPT can only be trusted up to approximately 0.5 GeV.

Finally, in Fig. 5 the phase shift  $\delta_1^1$  is shown below  $\sqrt{s} = 1.4$  GeV. This channel is dominated by the  $\rho(770)$  resonance, which was used in the determination of the low-energy constants for the IAM. However, it is observed that the IAM is not only consistent with the

experimental data close to the resonance mass, but also for energies rather far away from this resonance. Furthermore, for energies somewhat above 1 GeV the IAM to two loops improves the IAM to one loop, although inelastic effects should begin to be significant at these energies. As for ChPT, this only describes the low-energy tail of the  $\rho(770)$  resonance.

It has recently been shown that the IAM gives the correct analytical structure in the complex  $s$  plane [10]. Of course, this method produces the appropriate cuts on the first Riemann sheet, since these cuts are already present in ChPT. However, contrary to ChPT, the IAM can also produce poles on the second Riemann sheet, where resonances are related to such poles in the vicinity of the real axis. Indeed, the IAM gives the correct pole structure associated with the  $\rho(770)$  resonance. Furthermore, consistent with recent phenomenological analysis [31], this method also gives a pole in the  $I = 0$  S wave responsible for the strong final-state interaction in this channel. In fact, these poles have only been obtained for the IAM to one loop [10] but the same should also be true in general. Since this analytical structure is not trivial at all, this strongly supports the applicability of the IAM.

### III. PION FORM FACTORS

The pion vector form factor ( $F_V$ ) provides important information about the internal structure of the pion. Another quantity of interest is the pion scalar form factor ( $F_S$ ) defined by the matrix element of the quark density. These form factors depend on one kinematical variable  $s$ , giving by the square of the four-momentum transfer. They are analytical functions in the complex  $s$  plane with a unitarity cut starting at the  $\pi\pi$  threshold. The form factors will only be considered in the isospin limit, and the scalar form factor will be normalized according to  $F_S(0) = 1$ . Thus, they may be expanded around  $s = 0$  as

$$F(s) = 1 + \frac{1}{6}\langle r^2 \rangle s + cs^2 + \dots \quad (17)$$

where  $F$  is a generic symbol for the vector and scalar form factors. In the elastic region, one has the following unitarity relation

$$\text{Im}F(s) = \sigma(s)F^*(s)t_l^I(s), \quad (18)$$

which implies that the phase of  $F$  will coincide with the  $\pi\pi$  phase shift  $\delta_l^I$  in accordance with Watson's final-state theorem [32]. More precisely, in the elastic region the phase of  $F_V$  will coincide with the  $\pi\pi$   $I = 1$  P phase shift  $\delta_1^1$ , whereas the phase of  $F_S$  will be given by the  $I = 0$  S phase shift  $\delta_0^0$ . Above the  $K\bar{K}$  threshold, the elastic unitarity relation (18) has to be modified due to the important  $K\bar{K}$  inelasticity. This extended unitarity relation can be written as

$$\text{Im}F(s) = \sigma(s)F^*(s)t_l^I(s) + \sigma_{(K)}F_{(K)}^*(s)t_{l(K)}^I(s) \quad (19)$$

where  $F_{(K)}$  is the properly normalized kaon vector or scalar form factor. At still higher energies, other important inelastic channels must be included and the unitarity relation has to be generalized further.

### A. Chiral perturbation theory

The chiral expansion of the pion vector and scalar form factors can be written as

$$F(s) = F^{(0)}(s) + F^{(1)}(s) + F^{(2)}(s) + \dots \quad (20)$$

where  $F^{(n)}$  is of  $O(p^{2n})$ . Since the scalar form factor is normalized according to  $F_S(0) = 1$ , one has for the leading order term  $F^{(0)} = 1$  for both form factors. Regarding the one-loop correction  $F^{(1)}$ , this has been determined by Gasser and Leutwyler both in SU(2) ChPT [2] and in the SU(3) case [33].

For the two-loop correction  $F^{(2)}$ , this part has been evaluated by a dispersive analysis [13] in the elastic SU(2) approximation. This dispersive approach is based upon the two-loop perturbative interpretation of the elastic unitarity relation Eq. (18)

$$\begin{aligned} \text{Im}F^{(0)}(s) &= 0, \\ \text{Im}F^{(1)}(s) &= \sigma(s)t_l^{I(0)}(s), \\ \text{Im}F^{(2)}(s) &= \sigma(s) \left[ \text{Re}F^{(1)}(s)t_l^{I(0)}(s) + \text{Ret}_l^{I(1)}(s) \right]. \end{aligned} \quad (21)$$

These relations are satisfied for all energies above the  $\pi\pi$  threshold in the SU(2) approximation. Therefore, in this case the full two-loop pion form factors may be expressed in terms of a dispersion relation as [13]

$$F(s) = 1 + \frac{1}{6}\langle r^2 \rangle_S s + cs^2 + \frac{s^3}{\pi} \int_{4M_\pi^2}^{\infty} \frac{\sigma(s') \left\{ t_l^{I(0)}(s') \left[ 1 + \text{Re}F^{(1)}(s') \right] + \text{Ret}_l^{I(1)}(s') \right\} ds'}{s'^3(s' - s - i\epsilon)}. \quad (22)$$

For the vector form factor, the subtraction constants  $\langle r^2 \rangle$  and  $c$  can be written as

$$\begin{aligned} \langle r^2 \rangle_V &= \frac{1}{16\pi^2 F_\pi^2} \left[ (\bar{l}_6 - 1) + \frac{\bar{f}_1 M_\pi^2}{16\pi^2 F_\pi^2} \right], \\ c_V &= \frac{1}{16\pi^2 F_\pi^2} \left[ \frac{1}{60M_\pi^2} + \frac{\bar{f}_2}{16\pi^2 F_\pi^2} \right], \end{aligned} \quad (23)$$

whereas in the case of the scalar form factor, they may be expressed in the following way:

$$\begin{aligned} \langle r^2 \rangle_S &= \frac{3}{8\pi^2 F_\pi^2} \left[ (\bar{l}_4 - \frac{13}{12}) + \frac{\bar{d}_1 M_\pi^2}{16\pi^2 F_\pi^2} \right], \\ c_S &= \frac{1}{16\pi^2 F_\pi^2} \left[ \frac{19}{120M_\pi^2} + \frac{\bar{d}_2}{16\pi^2 F_\pi^2} \right]. \end{aligned} \quad (24)$$

The subtraction constants are given in terms of the scale-independent one-loop low-energy constants  $\bar{l}_4$  and  $\bar{l}_6$  and the additional two-loop coupling constants  $\bar{f}_1$ ,  $\bar{f}_2$ ,  $\bar{d}_1$ , and  $\bar{d}_2$ . These coupling constants could in the future be expressed in terms of chiral logs and two-loop renormalized chiral low-energy constants.

The dispersive analysis is not restricted to the elastic SU(2) approximation, but may be generalized to the inelastic case as well. The important  $K\bar{K}$  inelasticity can be included in this approach by considering the two-loop perturbative extended unitarity relations

$$\begin{aligned}
\text{Im}F^{(0)}(s) &= 0, \\
\text{Im}F^{(1)}(s) &= \sigma(s)t_l^{I(0)}(s) + \sigma_{(K)}(s)F_{(K)}^{(0)}(s)t_{l(K)}^{I(0)}(s), \\
\text{Im}F^{(2)}(s) &= \sigma(s) \left[ \text{Re}F^{(1)}(s)t_l^{I(0)}(s) + \text{Re}t_l^{I(1)}(s) \right] \\
&\quad + \sigma_{(K)}(s) \left[ \text{Re}F_{(K)}^{(1)}(s)t_{l(K)}^{I(0)}(s) + F_{(K)}^{(0)}(s)\text{Re}t_{l(K)}^{I(1)}(s) \right]. \tag{25}
\end{aligned}$$

In the inelastic case, these expressions have to be used above the  $K\bar{K}$  threshold in the dispersion relation Eq. (22). The other inelastic channels may also be included in the dispersive approach, but these will only be important somewhat above the  $K\bar{K}$  threshold.

## B. Inverse amplitude method

Also for the form factors, the elastic approximation will be used in the derivation of the IAM applied to two loops in the chiral expansion. However, some short remarks on the possible inclusion of inelasticities will also be given in this case.

### 1. Elastic approximation

The starting point for the IAM applied to the pion form factors is to write down a dispersion relation for the inverse of the form factor  $\Gamma = 1/F$ . In this dispersion relation, the elastic unitarity relation (18) gives  $\text{Im}\Gamma = -\text{Im}F/|F|^2 = -\sigma t/F$ . Unfortunately, this part cannot be computed exactly, as was the case for  $\pi\pi$  scattering, but it may be expanded to two-loop order in the chiral expansion  $\text{Im}\Gamma = -\sigma[t^{(0)}(1 - \text{Re}F^{(1)}) + \text{Re}t^{(1)}]$ . The subtraction constants can also be evaluated by expanding the function  $\Gamma$  to two-loop order as  $\Gamma = 1 - F^{(1)} + F^{(1)2} - F^{(2)}$ . Thus, neglecting any pole contribution arising from possible zeros in the form factors [6,7], the following dispersion relation is obtained for the IAM

$$\frac{1}{F(s)} = 1 + a_1s + a_2s^2 - \frac{s^3}{\pi} \int_{4M_\pi^2}^{\infty} \frac{\sigma(s') \left\{ t_l^{I(0)}(s') \left[ 1 - \text{Re}F^{(1)}(s') \right] + \text{Re}t_l^{I(1)}(s') \right\} ds'}{s'^3(s' - s - i\epsilon)}. \tag{26}$$

In order to simplify the connection between the IAM and two-loop ChPT, one can write down a dispersion relation for the function  $\Gamma^{(2)} = 1 - F^{(1)} + F^{(1)2} - F^{(2)}$ . Since this is the function  $\Gamma$  expanded to two-loop order in the chiral expansion, the subtraction constants in the dispersion relation for  $\Gamma^{(2)}$  will be the same as in Eq. (26). Furthermore, the perturbative elastic unitarity relations (21) give  $\text{Im}\Gamma^{(2)} = -\text{Im}F^{(1)} + 2\text{Re}F^{(1)}\text{Im}F^{(1)} - \text{Im}F^{(2)} = -\sigma t^{(0)} + \sigma 2\text{Re}F^{(1)}t^{(0)} - \sigma \text{Re}F^{(1)}t^{(0)} - \sigma \text{Re}t^{(1)} = -\sigma[t^{(0)}(1 - \text{Re}F^{(1)}) + \text{Re}t^{(1)}]$ , so the following dispersion relation is obtained for ChPT

$$\begin{aligned}
1 - F^{(1)}(s) + F^{(1)2}(s) - F^{(2)}(s) &= 1 + a_1s + a_2s^2 \\
- \frac{s^3}{\pi} \int_{4M_\pi^2}^{\infty} \frac{\sigma(s') \left\{ t_l^{I(0)}(s') \left[ 1 - \text{Re}F^{(1)}(s') \right] + \text{Re}t_l^{I(1)}(s') \right\} ds'}{s'^3(s' - s - i\epsilon)}. & \tag{27}
\end{aligned}$$

Since this is identical to Eq. (26), the IAM to two-loop order in the chiral expansion can be written as

$$F(s) = \frac{1}{1 - F^{(1)}(s) + F^{(1)2}(s) - F^{(2)}(s)}. \quad (28)$$

Even though the unitarity cut in the IAM for the pion form factors cannot be computed exactly, it is still expected that this method is superior to the truncation of the chiral expansion. This is based upon the fact that the expansion of  $t/F$  used in the IAM converges significantly faster than the corresponding expansion of  $F^*t$  used in ChPT. Actually, even the one-loop expansion  $t/F = t^{(0)}$  is a rather good approximation over a relatively large energy region [6]. With this approximation and the  $\pi\pi$  partial waves given by Eq. (14), the IAM to two loops will satisfy the elastic unitarity relation (18) exactly. Hence, the IAM is a rather consistent way of imposing the unitarity restriction on the chiral expansion.

The IAM was originally applied to the pion form factors in the one-loop approximation [6], which gives the result

$$F(s) = \frac{1}{1 - F^{(1)}(s)}. \quad (29)$$

With the  $\pi\pi$  partial waves given by Eq. (15), this form will also satisfy the elastic unitarity relation (18) exactly, provided that the one-loop approximation  $t/F = t^{(0)}$  is satisfied. However, in this case  $t/F$  and the subtraction constants are only expanded to one-loop order in the chiral expansion. Thus, even though the one-loop expansion of  $t/F$  is a rather good approximation, it is clear that the IAM to two loops will improve this approximation.

## 2. Inclusion of inelasticities

The first important inelastic channel is due to the  $K\bar{K}$  intermediate state. In order to include this inelastic channel in the IAM, the extended unitarity relation (19) has to be used above the  $K\bar{K}$  threshold. This gives  $\text{Im}\Gamma = -\text{Im}F/|F|^2 = -\sigma t/F - \sigma_{(K)}F_{(K)}^*t_{(K)}/|F|^2$ , which can be evaluated to two-loop order in the chiral expansion

$$\begin{aligned} \text{Im}\Gamma(s) &= -\sigma(s)\frac{t_l^I(s)}{F(s)} - \sigma_{(K)}(s)\frac{F_{(K)}^*(s)t_{l(K)}^I(s)}{|F(s)|^2} \\ &\approx -\sigma(s)\left\{t_l^{I(0)}(s)\left[1 - \text{Re}F^{(1)}(s)\right] + \text{Re}t_l^{I(1)}(s)\right\} \\ &\quad -\sigma_{(K)}(s)\left\{t_{l(K)}^{I(0)}(s)\left[F_{(K)}^{(0)}(s) - 2F_{(K)}^{(0)}(s)\text{Re}F^{(1)}(s)\right.\right. \\ &\quad \left.\left.+ \text{Re}F_{(K)}^{(1)}(s)\right] + F_{(K)}^{(0)}(s)\text{Re}t_{l(K)}^{I(1)}(s)\right\}. \end{aligned} \quad (30)$$

This expression has to be used above the  $K\bar{K}$  threshold in the dispersion relation (26) for the IAM. In order to simplify the relation between the IAM and ChPT in this inelastic case, the perturbative extended unitarity relations (25) may be used to evaluate  $\text{Im}\Gamma^{(2)}$  to two-loop order in the chiral expansion. Since this will give an expression exactly similar to Eq. (30), the inelastic IAM to two loops can also be written in the form (28) with the  $K\bar{K}$  inelasticity included in ChPT. In the same way, by expanding to one-loop order in the chiral expansion, the inelastic IAM to one loop will be given by a form similar to Eq. (29). As was the case in the elastic approximation, it is also expected that the inelastic higher order corrections are substantially more suppressed for the IAM than for ChPT. However, it still has to be investigated whether the IAM is actually able to correctly describe the  $K\bar{K}$  and other inelasticities.

### C. Comparison with experiment

The pion vector form factor is well known experimentally both in the time-like region  $s > 4M_\pi^2$  [34] and in the space-like region  $s < 0$  GeV<sup>2</sup> [35,36]. As for the scalar form factor, this is not directly accessible to experiment. However, it has been determined in terms of the experimental phase shifts for the  $\pi\pi/K\bar{K}$  system by a dispersive analysis [13,37]. In the following, the theoretical form factors will be limited to the elastic approximation when compared to the experimental information.

#### 1. Vector form factor

The vector form factor to one loop depends on the single scale-independent low-energy constant  $\bar{l}_6$ . This can be fixed for both ChPT and the IAM from the experimental value of the pion charge radius  $\langle r^2 \rangle_V = 0.439 \pm 0.008$  fm<sup>2</sup> [35]. With the central experimental value, one obtains the results for  $\bar{l}_6$  displayed in the first and third column in Table III, which is consistent with independent information on this low-energy constant [9]. For two-loop ChPT, the value of  $\bar{l}_6$  should in principle be re-evaluated taking into account the two-loop corrections. However, since a thorough re-evaluation seems rather out of reach at the moment, the one-loop value of  $\bar{l}_6$  is also used in two-loop ChPT. Therefore, from the central experimental value of the pion charge radius [35], one obtains the result that the two-loop contribution to  $\langle r^2 \rangle_V$  contained in the coupling constant  $\bar{f}_1$  vanishes. For the other coupling constant  $\bar{f}_2$ , this can be fixed from the value  $c_V = 4.1$  GeV<sup>-4</sup> [13] with a result displayed in the second column in Table III. Finally, for the renormalized low-energy constants  $l_1^r$ ,  $l_2^r$ ,  $l_3^r$ , and  $l_4^r$  occurring in the  $\pi\pi$  partial waves to one loop, they will be given by the values shown in the second column in Table I.

For the IAM to two loops, the low-energy constant  $\bar{l}_6$  and the coupling constants  $\bar{f}_1$  and  $\bar{f}_2$  may be determined simultaneously by fitting the time-like experimental data below  $\sqrt{s} = 0.9$  GeV [34] together with the space-like experimental data [35]. For the other renormalized low-energy constants  $l_1^r$ ,  $l_2^r$ ,  $l_3^r$ , and  $l_4^r$ , the values shown in the fourth column in Table I are used. This gives a rather good fit with values of  $\bar{l}_6$ ,  $\bar{f}_1$ , and  $\bar{f}_2$  displayed in the fourth column in Table III. For the the pion charge radius  $\langle r^2 \rangle_V$  and the low-energy parameter  $c_V$  also shown in Table III, it is observed the the predictions for the IAM to two loops agree remarkably well with the experimental information  $\langle r^2 \rangle_V = 0.439 \pm 0.008$  fm<sup>2</sup> [35] and  $c_V = 4.1$  GeV<sup>-4</sup> [13]. In addition, with this method one finds that the two-loop correction to  $\langle r^2 \rangle_V$  contained in the coupling constant  $\bar{f}_1$  is approximately 20% of the one-loop contribution, which is quite reasonable. From Table III, it is furthermore observed that the prediction for  $c_V$  obtained from the IAM to one loop also agrees remarkably well with the experimental information, whereas the corresponding prediction obtained from one-loop ChPT is far too small.

The vector form factor  $|F_V|^2$  is shown for  $-1$  GeV<sup>2</sup>  $\leq s \leq 1$  GeV<sup>2</sup> in Fig. 6. The IAM to two loops describes the data very well both in the time-like and in the space-like regions. In fact, also the space-like data for  $s < -0.26$  GeV<sup>2</sup> [36], which were not included in the fit, agree well with the IAM to two loops. Of course, the small isospin violating  $\rho - \omega$  mixing is not reproduced by this method, since the isospin limit has been applied throughout this paper. In addition, this method should only be reliable below approximately  $s = 1$  GeV<sup>2</sup>,

since the elastic approximation has been used for the vector form factor. As for the IAM to one loop, this agrees well with the space-like experimental data. However, in the time-like region this method only approximates the  $\rho(770)$  resonance, as has been discussed in greater detail in Ref. [9]. Nevertheless, it is obvious that the IAM to both one and two loops significantly improves the behavior of ChPT, which only accounts for the low-energy tail of the  $\rho(770)$  resonance. The agreement between one and two-loop ChPT and the space-like experimental data [35] can be slightly improved by fitting these experimental data [38], but this will not change the range of applicability of ChPT significantly.

In Fig. 7, the predictions for the phase  $\delta_1^1$  are shown below  $\sqrt{s} = 1$  GeV. Only the IAM are shown since one and two-loop ChPT will give the chiral  $\pi\pi$  I=1 P phase shifts to leading and one-loop order respectively. For the IAM to two loops, the phase agrees very well with the experimental data and gives a resonance at  $M_\rho = 0.771$  GeV defined to be at  $\delta_1^1(M_\rho) = \pi/2$ . Furthermore, since this method also agrees well with the results of the IAM for the  $\pi\pi$  I=1 P phase shifts shown in Fig. 5, the IAM to two loops satisfies the elastic unitarity relation (18) very well indeed. As for the IAM to one loop, since this only approximates the experimental data, the elastic unitarity relation (18) will be somewhat violated in this case. However, the IAM to one loop is also quite consistent with a resonance structure [39] and will give a resonance at  $M_\rho = 0.734$  GeV. Thus, the IAM to both one and two loops are rather consistent approaches to extend the range of applicability of ChPT in the case of the vector form factor.

## 2. Scalar form factor

The normalized scalar form factor to one loop is given in terms of the single scale-independent low-energy constant  $\bar{l}_4$ . The same low-energy constant also occurs in  $\pi\pi$  scattering to one loop, where the central value  $l_4^r(M_\rho) = 5.60 \times 10^{-3}$  obtained from the ratio  $F_K/F_\pi$  [2,33] was used. Changing to scale-independent low-energy constants [2] gives  $\bar{l}_4 = 4.30$ , which is used both in ChPT and the IAM to one loop. The same value of  $\bar{l}_4$  is also used in two-loop ChPT, whereas the coupling constants  $\bar{d}_1$  and  $\bar{d}_2$  are determined from the values  $\langle r^2 \rangle_S = 0.60$  fm<sup>2</sup> and  $c_S = 10.6$  GeV<sup>-4</sup> [13,37], respectively. For the additional low-energy constants to two loops  $l_1^r$ ,  $l_2^r$ , and  $l_3^r$ , they will be given by the values shown in the second column in Table I.

For the IAM to two loops, the low-energy constant  $\bar{l}_4$  and the coupling constants  $\bar{d}_1$  and  $\bar{d}_2$  cannot be determined in the same way as was applied for the vector form factor. This is because the scalar form factor is not directly accessible to experiment. However, in the elastic region the phase of the scalar form factor is given by the  $\pi\pi$  I=0 S phase shift, which is known experimentally. Therefore, the coupling constants  $\bar{d}_1$  and  $\bar{d}_2$  may be determined by fitting the experimental phase shift  $\delta_0^0$  below  $\sqrt{s} = 0.9$  GeV [19–22], whereas  $\bar{l}_4$  can be fixed from the requirement  $\langle r^2 \rangle_S = 0.60$  fm<sup>2</sup>. With the remaining low-energy constants  $l_1^r$ ,  $l_2^r$ , and  $l_3^r$  given by the values in the fourth column in Table I, this gives an acceptable fit for the  $\pi\pi$  I=0 S phase shift.

In Table IV, the results for the low-energy constant  $\bar{l}_4$  and the coupling constants  $\bar{d}_1$  and  $\bar{d}_2$  are shown both for ChPT and the IAM. As for the IAM to two loops, the value of  $\bar{l}_4$  is slightly different from the one-loop value  $\bar{l}_4 = 4.30$ . This might well be due to the inclusion of the higher order corrections in the determination of this low-energy constant in



the two-loop case. However, the value of  $\bar{l}_4$  for the IAM to two loops is still consistent with the value  $\bar{l}_4 = 4.3 \pm 0.9$  obtained from the ratio  $F_K/F_\pi$  to one-loop order in ChPT [2,33]. In fact, using the value  $\bar{l}_4 = 3.68$  in the IAM to two loops, the previous numerical analysis of  $\pi\pi$  scattering and the pion vector form factor will only change insignificantly. The largest numerical difference will be for the  $\pi\pi$  threshold parameters, but the values given for the IAM to two loops in Table II will at most change by 5%. In the future it might be possible to determine the two-loop value of  $\bar{l}_4$  from independent observables.

The corresponding values of the pion scalar radius  $\langle r^2 \rangle_S$  and the low-energy parameter  $c_S$  are also given in Table IV. For the pion scalar radius, the predictions obtained from ChPT and the IAM to one loop agree rather well with the result from the dispersive analysis  $\langle r^2 \rangle_S = 0.60 \text{ fm}^2$  (solution B) [13,37]. For the low-energy parameter  $c_S$ , the predictions from the IAM to one and two loops agree within 10-15% with the result  $c_S = 10.6 \text{ GeV}^{-4}$  (solution B) [13,37], whereas the corresponding prediction from one-loop ChPT is too small.

The scalar form factor is known up to  $\sqrt{s} = 0.7 \text{ GeV}$  from the dispersive analysis in Refs. [13,37]. In Fig. 8, solution B from this dispersive analysis is compared to the scalar form factor obtained from the IAM and ChPT. It is observed that the IAM to two loops agrees very well with the dispersive analysis over the whole energy region, whereas the same is only true for the IAM to one loop below approximately 0.5 GeV. As for two-loop ChPT, this works rather well up to about 0.4 GeV, while one-loop ChPT only agrees with the dispersive analysis below the  $\pi\pi$  threshold. This is due to the strong final-state interaction, which makes the higher order corrections important even at low energies.

In Fig. 9, the phase  $\delta_0^0$  obtained from the IAM is shown below  $\sqrt{s} = 1 \text{ GeV}$ . For the IAM to two loops, it is observed that below approximately 0.9 GeV, the phase agrees rather well with both the experimental data and the two-loop IAM result for the  $\pi\pi$  I=0 S phase shift shown in Fig. 3. Thus, the IAM to two loops satisfies the elastic unitarity relation (18) rather well. Slightly above 0.9 GeV, the IAM to two loops shows a very rapid phase variation of approximately  $180^\circ$ , which might be a signal indicating that this method could reproduce the  $f_0(980)$  resonance. However, in order to investigate this the  $K\bar{K}$  inelasticity must be included in the IAM. As for the IAM to one loop, this method only describes the data well at rather low energies. The agreement could be improved at somewhat higher energies by reducing the value of the low-energy constant  $\bar{l}_4$  within the error bars  $\bar{l}_4 = 4.3 \pm 0.9$ , but this will at the same time give a value for the pion scalar radius less consistent with the dispersive result  $\langle r^2 \rangle_S = 0.60 \text{ fm}^2$ .

Finally, the phase difference  $\delta_0^0 - \delta_1^1$  between the scalar and vector form factors is shown in Fig. 10 below  $\sqrt{s} = 0.38 \text{ GeV}$ . The IAM to two loops agrees very well with both the central experimental data and the results of the IAM for the  $\pi\pi$  phase shift difference shown in Fig. 2. The IAM to one loop also agrees with the experimental data within the error bars, but is slightly different from the corresponding phase shift differences shown in Fig. 2. As already pointed out, it is expected that forthcoming kaon facilities like DAΦNE can reduce the error bars on  $\delta_0^0 - \delta_1^1$  significantly [30], which will allow one to test the consistency of the IAM at low energies in greater detail.

## IV. CONCLUSIONS

The IAM is based upon the use of unitarity and dispersion relations together with the chiral expansion. It has previously been shown that this method applied to one-loop order successfully extends the range of applicability of ChPT. However, the IAM is not restricted to the one-loop approximation but can in general be applied to any given order in the chiral expansion. In the present paper, the extension of the IAM to two loops has been analysed in the case of  $\pi\pi$  scattering and the pion form factors. The analysis has mainly been restricted to the elastic approximation but the possible extension to the inelastic case has also been discussed in some detail.

From the derivation of the IAM applied to two loops in the chiral expansion, it is found that this approach indeed improves the IAM to one loop both for  $\pi\pi$  scattering and in the case of the pion form factors. For  $\pi\pi$  scattering, a comparison with the experimental data shows that the IAM applied to two loops is in fact rather consistent with the experimental data up to energies where inelasticities become essential. At somewhat lower energies, the two-loop approach compares well with the one-loop approximation, and in the threshold region they both agree with ChPT. In the case of the pion form factors, it is also found that the IAM to two loops is consistent with the experimental information up to the first important inelastic threshold. For the IAM to one loop, although this also successfully extends the range of applicability of ChPT, it only approximates the form factors at higher energies.

Thus, the present analysis suggests that the IAM is indeed a rather systematic way of extending the range of applicability of ChPT. However, in order to investigate this in greater detail, the IAM to two loops should be applied to other processes. In this way, some of the two-loop low-energy constants in the IAM might be determined from independent observables. There are also other ways of extending the range of applicability of ChPT and work is still in progress in this subject. However, at present the IAM provides one of the most intriguing methods to improve ChPT in a systematic manner.

## ACKNOWLEDGMENTS

The author thanks A. Miranda and G. C. Oades for discussions and comments, and J. Bijnens for a private communication regarding the two-loop low-energy constants estimated from resonance exchange. The support from The Faculty of Science, Aarhus University is also acknowledged.

## REFERENCES

- [1] S. Weinberg, *Physica* **96A**, 327 (1979).
- [2] J. Gasser and H. Leutwyler, *Ann. Phys. (N.Y.)* **158**, 142 (1984); *Nucl. Phys.* **B250**, 465 (1985).
- [3] H. Leutwyler, *Ann. Phys. (N.Y.)* **235**, 165 (1994).
- [4] J. Bijnens, G. Colangelo, and J. Gasser, *Nucl. Phys.* **B427**, 427 (1994).
- [5] H. W. Fearing and S. Scherer, *Phys. Rev. D* **53**, 315 (1996).
- [6] T. N. Truong, *Phys. Rev. Lett.* **61**, 2526 (1988).
- [7] A. Dobado, M. J. Herrero, and T. N. Truong, *Phys. Lett. B* **235**, 134 (1990); T. N. Truong, *Phys. Rev. Lett.* **67**, 2260 (1991); A. Dobado and J. R. Peláez, *Phys. Rev. D* **47**, 4883 (1993); *Z. Phys. C* **57**, 501 (1993).
- [8] T. Hannah, *Phys. Rev. D* **51**, 103 (1995); **52**, 4971 (1995).
- [9] T. Hannah, *Phys. Rev. D* **54**, 4648 (1996).
- [10] A. Dobado and J. R. Peláez, “The inverse amplitude method in Chiral Perturbation Theory,” Report No. hep-ph/9604416.
- [11] M. Knecht *et al.*, *Nucl. Phys.* **B457**, 513 (1995).
- [12] J. Bijnens *et al.*, *Phys. Lett. B* **374**, 210 (1996).
- [13] J. Gasser and U. G. Meissner, *Nucl. Phys.* **B357**, 90 (1991).
- [14] M. Alston-Garnjost *et al.*, *Phys. Lett.* **36B**, 152 (1971).
- [15] S. Weinberg, *Phys. Rev. Lett.* **17**, 616 (1966).
- [16] V. Bernard, N. Kaiser, and U. G. Meissner, *Nucl. Phys.* **B357**, 129 (1991).
- [17] G. Ecker *et al.*, *Nucl. Phys.* **B321**, 311 (1989); G. Ecker *et al.*, *Phys. Lett. B* **223**, 425 (1989).
- [18] J. Bijnens, (private communication).
- [19] L. Rossetti *et al.*, *Phys. Rev. D* **15**, 574 (1977).
- [20] S. D. Protopopescu *et al.*, *Phys. Rev. D* **7**, 1279 (1973).
- [21] B. Hyams *et al.*, *Nucl. Phys.* **B64**, 134 (1973); W. Ochs, thesis, Ludwig-Maximilians-Universität, 1973 (unpublished).
- [22] P. Estabrooks and A. D. Martin, *Nucl. Phys.* **B79**, 301 (1974).
- [23] M. J. Losty *et al.*, *Nucl. Phys.* **B69**, 185 (1974).
- [24] W. Hoogland *et al.*, *Nucl. Phys.* **B126**, 109 (1977).
- [25] D. Morgan and M. R. Pennington, in *The Second DAΦNE Physics Handbook*, edited by L. Maiani, G. Pancheri, and N. Paver (INFN, Frascati, 1995), Vol. 1, p. 193.
- [26] M. M. Nagels *et al.*, *Nucl. Phys.* **B147**, 189 (1979).
- [27] B. Ananthanarayan, D. Toublan, and G. Wanders, *Phys. Rev. D* **53**, 2362 (1996).
- [28] B. Adeva *et al.*, “Lifetime measurement of  $\pi^+\pi^-$  atoms to test low-energy QCD predictions,” Report No. CERN/SPSLC 95-1.
- [29] J. Gasser and U. G. Meissner, *Phys. Lett. B* **258**, 219 (1991).
- [30] M. Baillargeon and P. J. Franzini, in *The Second DAΦNE Physics Handbook*, edited by L. Maiani, G. Pancheri, and N. Paver (INFN, Frascati, 1995), Vol. 1, p. 413.
- [31] Particle Data Group, R. M. Barnett *et al.*, *Phys. Rev. D* **54**, 1 (1996).
- [32] K. M. Watson, *Phys. Rev.* **95**, 228 (1954).
- [33] J. Gasser and H. Leutwyler, *Nucl. Phys.* **B250**, 517 (1985).
- [34] L. M. Barkov *et al.*, *Nucl. Phys.* **B256**, 365 (1985); L. M. Kurdadze *et al.*, *Yad. Fiz.* **40**, 451 (1984) [*Sov. J. Nucl. Phys.* **40**, 286 (1984)]; G. V. Anikin *et al.*, Report No.

- INP 83-85 (unpublished); S. R. Amendolia *et al.*, Phys. Lett. **138B**, 454 (1984); I. B. Vasserman *et al.*, Yad. Fiz. **33**, 709 (1981) [Sov. J. Nucl. Phys. **33**, 368 (1981)]; A. Quenzer *et al.*, Phys. Lett. **76B**, 512 (1978).
- [35] NA7 Collaboration, S. R. Amendolia *et al.*, Nucl. Phys. **B277**, 168 (1986).
- [36] C. J. Bebek *et al.*, Phys. Rev. D **17**, 1693 (1978).
- [37] J. F. Donoghue, J. Gasser, and H. Leutwyler, Nucl. Phys. **B343**, 341 (1990).
- [38] J. Bijnens and F. Cornet, Nucl. Phys. **B296**, 557 (1988); G. Colangelo, M. Finkemeier, and R. Urech, Phys. Rev. D **54**, 4403 (1996).
- [39] L. V. Dung and T. N. Truong, “Equivalence Between Vector Meson Dominance and Unitarised Chiral Perturbation Theory,” Report No. hep-ph/9607378.

## TABLES

TABLE I. Values of the low-energy constants at the  $\rho(770)$  scale used for one-loop ChPT (ChPT1), two-loop ChPT (ChPT2), the IAM to one loop (IAM1), and the IAM to two loops (IAM2). For a discussion on how these low-energy constants have been determined see the text.

	ChPT1	ChPT2	IAM1	IAM2
$10^3 l_1^r(M_\rho)$	-5.40	-5.40	-4.13	-3.57
$10^3 l_2^r(M_\rho)$	5.67	5.67	4.05	1.21
$10^3 l_3^r(M_\rho)$	0.82	0.82	0.82	0.82
$10^3 l_4^r(M_\rho)$	5.60	5.60	5.60	5.60
$10^5 r_1^r(M_\rho)$		-6.1		-6.1
$10^5 r_2^r(M_\rho)$		13.0		13.0
$10^5 r_3^r(M_\rho)$		-17.0		-17.0
$10^5 r_4^r(M_\rho)$		-10.1		-10.1
$10^5 r_5^r(M_\rho)$		11.4		16.9
$10^5 r_6^r(M_\rho)$		3.0		-6.5

TABLE II. Threshold parameters obtained from current algebra (CA), one-loop ChPT (ChPT1), two-loop ChPT (ChPT2), the IAM to one loop (IAM1), and the IAM to two loops (IAM2). The experimental data are from Ref. [26] except for  $b_1^1$ , which is from Ref. [27].

	CA	ChPT1	ChPT2	IAM1	IAM2	Experiment
$2a_0^0 - 5a_0^2$	0.545	0.623	0.654	0.659	0.665	$0.657 \pm 0.052$
$a_0^0$	0.159	0.205	0.222	0.222	0.221	$0.26 \pm 0.05$
$b_0^0$	0.182	0.254	0.282	0.283	0.278	$0.25 \pm 0.03$
$-10a_0^2$	0.454	0.425	0.420	0.429	0.447	$0.28 \pm 0.12$
$-10b_0^2$	0.908	0.736	0.727	0.768	0.809	$0.82 \pm 0.08$
$10a_1^1$	0.303	0.378	0.405	0.383	0.375	$0.38 \pm 0.02$
$10^2 b_1^1$		0.502	0.830	0.622	0.494	$0.6 \pm 0.4$

TABLE III. Values of the scale-independent low-energy constant  $\bar{l}_6$  and the coupling constants  $\bar{f}_1$  and  $\bar{f}_2$  together with the corresponding values of the pion charge radius  $\langle r^2 \rangle_V$  and the low-energy parameter  $c_V$ . The notation is as in Table I.

	ChPT1	ChPT2	IAM1	IAM2
$\bar{l}_6$	16.20	16.20	16.20	13.19
$\bar{f}_1$		0.0		197.3
$\bar{f}_2$		6.3		3.7
$\langle r^2 \rangle_V$ (fm <sup>2</sup> )	0.439	0.439	0.439	0.434
$c_V$ (GeV <sup>-4</sup> )	0.6	4.1	4.2	3.9

TABLE IV. Values of the scale-independent low-energy constant  $\bar{l}_4$  and the coupling constants  $\bar{d}_1$  and  $\bar{d}_2$  together with the corresponding values of the pion scalar radius  $\langle r^2 \rangle_S$  and the low-energy parameter  $c_S$ . The notation is as in Table I.

	ChPT1	ChPT2	IAM1	IAM2
$\bar{l}_4$	4.30	4.30	4.30	3.68
$\bar{d}_1$		17.0		59.8
$\bar{d}_2$		8.3		6.0
$\langle r^2 \rangle_S$ (fm <sup>2</sup> )	0.56	0.60	0.56	0.60
$c_S$ (GeV <sup>-4</sup> )	6.0	10.6	11.7	12.2

## FIGURES

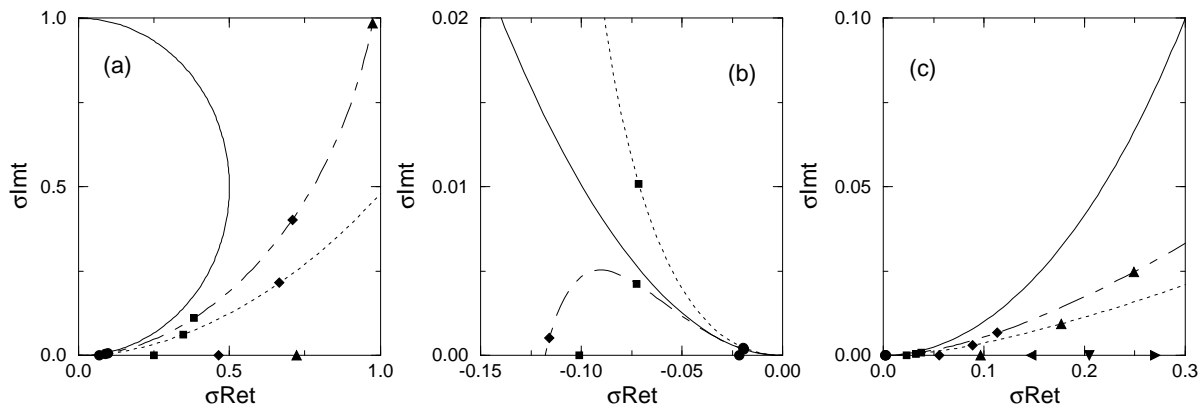


FIG. 1. Argand diagrams for the ChPT partial waves  $t_0^0$  (a),  $t_0^2$  (b), and  $t_1^1$  (c), respectively. The solid line is the unitarity circle, the dashed-dotted line two-loop ChPT, and the dotted line one-loop ChPT. The leading order current algebra result lies on the real axis of the diagrams. The corresponding energies are displayed on the curves for 0.3 GeV (circles), 0.4 GeV (squares), 0.5 GeV (diamonds), 0.6 GeV (up triangles), 0.7 GeV (left triangles), 0.8 GeV (down triangles), and 0.9 GeV (right triangles).

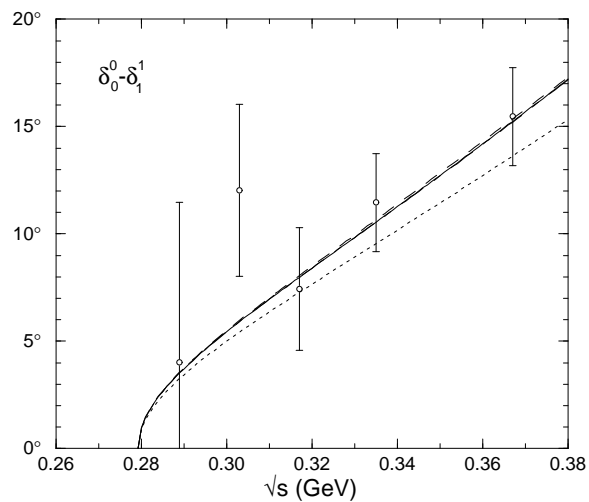


FIG. 2. The phase shift difference  $\delta_0^0 - \delta_1^1$  below  $\sqrt{s} = 0.38$  GeV. The solid line is the IAM to two loops, the dashed line the IAM to one loop, the dashed-dotted line two-loop ChPT, and the dotted line one-loop ChPT. The solid, dashed, and dashed-dotted curves are very close to each other and therefore hard to distinguish from each other in the figure. The experimental data are from Ref. [19].

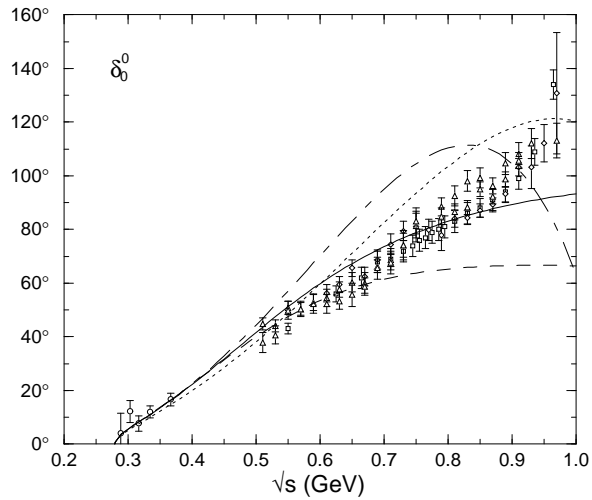


FIG. 3. The phase shift  $\delta_0^0$  below  $\sqrt{s} = 1$  GeV. The curves are as in Fig. 2 and the experimental data are from Ref. [19] (circles), Ref. [20] (squares), Ref. [21] (diamonds), and Ref. [22] (triangles).

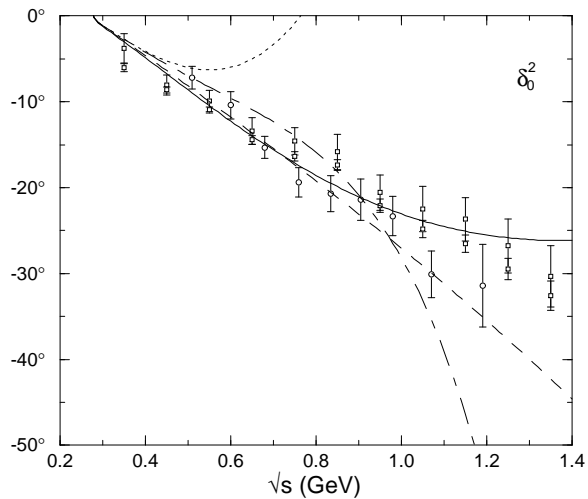


FIG. 4. The phase shift  $\delta_0^2$  below  $\sqrt{s} = 1.4$  GeV. The curves are as in Fig. 2 and the experimental data are from Ref. [23] (circles) and Ref. [24] (squares).



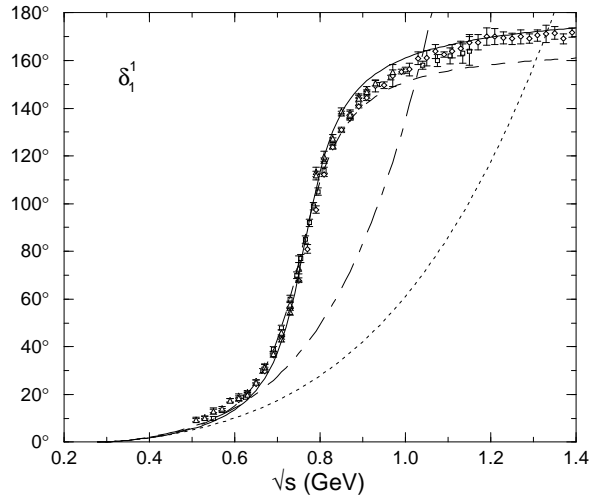


FIG. 5. The phase shift  $\delta_1^1$  below  $\sqrt{s} = 1.4$  GeV. The curves are as in Fig. 2 and the experimental data are from Ref. [20] (squares), Ref. [21] (diamonds), and Ref. [22] (triangles).

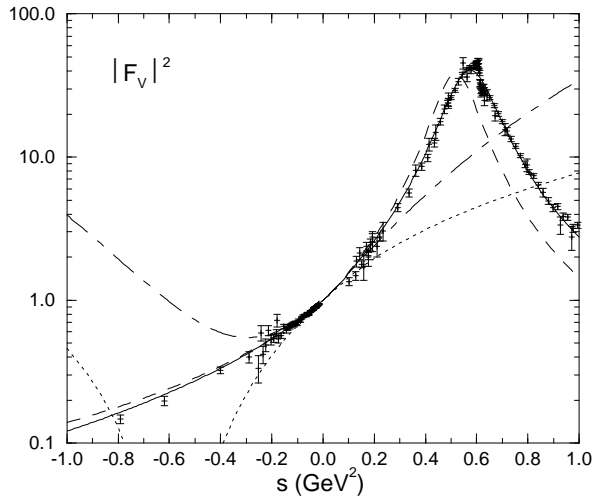


FIG. 6. The vector form factor  $|F_V|^2$  for  $-1 \text{ GeV}^2 \leq s \leq 1 \text{ GeV}^2$ . The curves are as in Fig. 2 and the experimental data are from Ref. [34], Ref. [35], and Ref. [36].

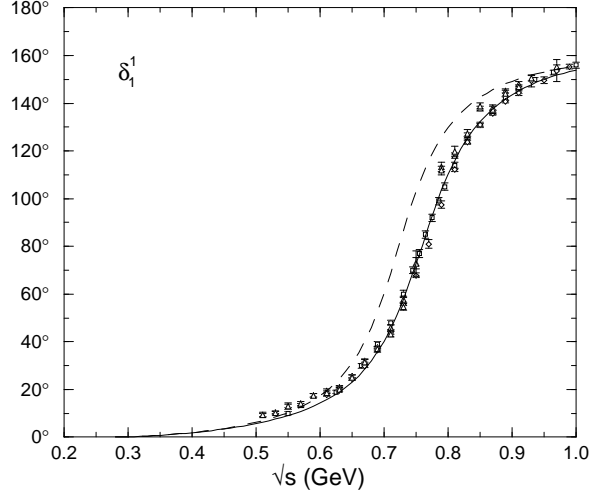


FIG. 7. The phase  $\delta_1^1$  for the vector form factor below  $\sqrt{s} = 1$  GeV. The solid line is the IAM to two loops, the dashed line the IAM to one loop, and the experimental data are as in Fig. 5.

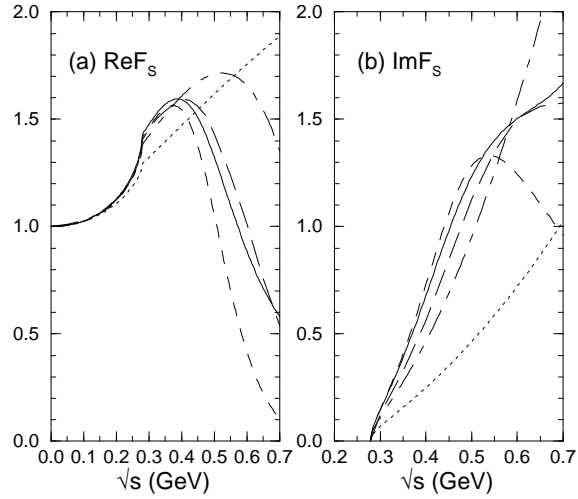


FIG. 8. The real (a) and imaginary (b) part of the scalar form factor  $F_S$  below  $\sqrt{s} = 0.7$  GeV. The long-dashed curve is solution B from a dispersive analysis [13,37], whereas the other curves are as in Fig. 2.

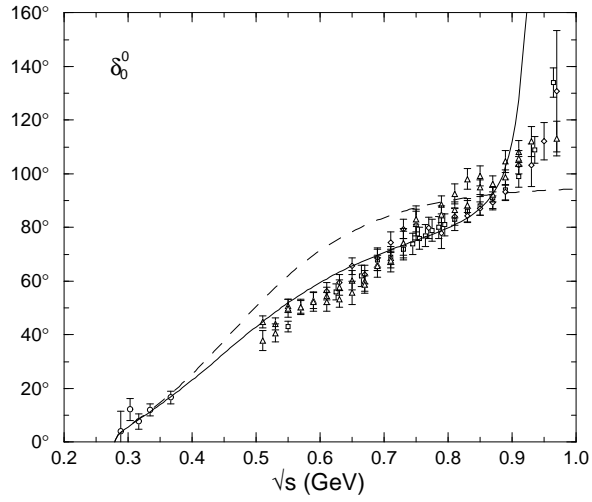


FIG. 9. The phase  $\delta_0^0$  for the scalar form factor below  $\sqrt{s} = 1$  GeV. The curves are as in Fig. 7 and the experimental data are as in Fig. 3.

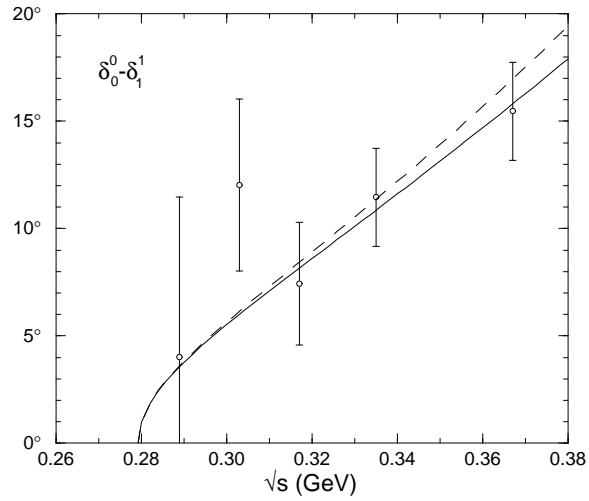


FIG. 10. The phase difference  $\delta_0^0 - \delta_1^1$  between the scalar and vector form factors below  $\sqrt{s} = 0.38$  GeV. The curves are as in Fig. 7 and the experimental data are as in Fig. 2.